crystals

MDPI

Article

A Newly Synthesized Heterobimetallic Ni^{II}-Gd^{III} Salamo-BDC-Based Coordination Polymer: Structural Characterization, DFT Calculation, Fluorescent and Antibacterial Properties

Yong-Fan Cui, Yu Zhang, Ke-Feng Xie and Wen-Kui Dong *

School of Chemical and Biological Engineering, Lanzhou Jiaotong University, Lanzhou 730070, Gansu, China; SZS18794249760@163.com (Y.-F.C.); 18394178640@163.com (Y.Z.); xiekefeng@mail.lzjtu.cn (K.-F.X.)

* Correspondence: dongwk@mail.lzjtu.cn

Received: 25 October 2019; Accepted: 12 November 2019; Published: 14 November 2019

Abstract: A unprecedented hetero-bimetallic 3d-4f BDC-salamo-based coordination polymer, [(L)Ni(BDC)Gd(NO_3)(DMF)] was prepared and validated via elemental analyses, IR and UV–Visible absorption spectra, DFT calculation, and X-ray crystallography. The six-coordinated Ni1 ion lies at the N_2O_2 donor site of the L^{2-} moiety, and one DMF O atom and carboxylate O atom occupy, collectively, the axial positions, and form a twisted octahedron. The nine-coordinated Gd1 ion consists of three oxygen atoms (O12, O13, and O14) of two carboxylate groups, two oxygen atoms (O8 and O9) derived from one bidentate nitrate group, and an O_2O_2 coordination site (O1, O2, O6, and O5) of the L^{2-} unit, forming a twisted three-capped triangular prism coordination geometry. Compared to the ligand (H_2L), the fluorescence intensity decreases due to the coordination of metal ions. Meanwhile, the antibacterial activities are researched.

Keywords: 3d-4f coordination polymer; salamo-based ligand; crystal structure; property; DFT calculation

1. Introduction

The salen-like compounds are an important class of Schiff bases having a C_2 axis of symmetry [1–5], and the coordinating group of the salen-like ligands mostly contain two Schiff base N and phenol O atoms on the skeleton [6–11] which constitutes a tetradentate N_2O_2 coordination cavity, and is easy to bind with transition metal ions, alkaline earth metal ions, and rare earth metal ions to obtain various metal complexes such as mononuclear, binuclear, multinuclear, and heteropolynuclear complexes [12–17]. Salen and its metal complexes have been researched far and wide [18–23] for their excellent catalytic [24,25] and biological activities [26–28], magnetic materials [29–33], electrochemical researches [34–37], supramolecular buildings [38–42], and fluorescence properties [43–46]. The salamo-like ligands are a very important kind of versatile chelating bisoxime ligands including N_2O_2-donor cavity [47]. These ligands are synthesized by structural modification of the salen-like ligands, and are generally coordinated with metal ions to obtain multinuclear metal complexes. On account of the high coordination abilities of the phenoxy atoms, many central metal ions could be coordinated to prepare heteromultinuclear metal complexes [48–50]. However, transition metal complexes of salamo-based compounds have aroused wide concern on their photophysical properties and reported successively [51–57], and heterobimetallic 3d-4f salamo-like complexes, especially containing auxiliary ligands, have rarely been reported [58]. It is generally true that the self-assembly process of organometallic complexes is frequently used to construct metal organic framework (MOF) materials [59]. Here, an unprecedented heterobimetallic salamo-like coordination

polymer, $_{\infty}$[(L)Ni(BDC)Gd(NO_3)(DMF)], is synthesized, and the photophysical characteristics and antibacterial activities of H_2L and its Ni^{II}-Gd^{III} polymer are discussed. In addition, the paper also introduces DFT calculations to study the electronic structure and properties of the polymer.

2. Experimental Section

2.1. Materials and Physical Measurements

3-Ethoxybenzaldehyde (97%) was bought from Alfa Aesar and utilized without further purification. Terephthalic acid (BDC) and other analytically pure solvents and reagents were from Tianjin Chemical Reagent Factory. Elemental analyses were detected with an IRIS ER/S-WP-1 ICP atomic emission spectrometer and GmbH VarioEL V3.00 automatic elemental analysis instrument from Berlin, Germany, respectively. Melting points were measured via a micro melting point apparatus manufactured by Beijing Taike Instrument Limited company and were uncorrected. FT-IR spectra were recorded on a Vertex70 FT-IR spectrophotometer, with samples prepared as KBr (500–4000 cm^{-1}) from Bruker, Germany. UV-vis spectra were obtained on a Shimadzu UV-3900 spectrometer from Hitachi, Tokyo, Japan. Fluorescence spectra were obtained on a F-7000 FL 220-240V spectrophotometer from Hitachi, Tokyo, Japan. ^{1}H NMR spectra were determined by a German Bruker AVANCE DRX-400 spectrometer. X-ray structure determination was carried out on a SuperNova Dual (Cu at zero) Eos four-circle diffractometer (Bruker, Germany) and Mo-Kα (λ = 0.71073 Å) ray radiation was monochromated with graphite [60]. Molecular orbital calculations were performed by density functional theory (DFT). The DFT methods used were the gradient-corrected functional proposed by B3LYP; basis sets with SDD were used to expand the Kohn–Sham orbitals. These calculations were done using the Gaussian 09 (Shenzhen, P. R. China.) suite of programs. The conductivity was measured by DOS-110 conductivity meter produced by Shanghai Precision Scientific Instrument Co., Ltd. Powder X-ray diffraction (PXRD) data were recorded on a Rigaku D/Max-2400 X-ray diffractometer with Cu/Kα as the radiation source (λ = 0.15406 nm) in the angular range 2θ = 5–50° at room temperature.

2.2. Preparation and Characterization of H_2L

H_2L was prepared in the light of a similar method previously reported [61]. The synthetic route to H_2L is shown in Scheme 1. An ethanol solution (10 mL) of 1,2-bis(aminooxy)ethane (276.0 mg, 3.0 mmol) was added to an ethanol solution (20 mL) of 2-hydroxy-3-ethoxybenzaldehyde (996.0 mg, 6.0 mmol), and the mixture was stirred at 60~55 °C for 5 h. Then, white crystalline H_2L was separated and obtained. Yield: 784.0 mg, 67.3%. m.p. 462~463 K. Anal. calcd for $C_{20}H_{24}N_2O_6$ (%): C, 61.84; H, 6.23; N, 7.21. Found (%): C, 61.80; H, 6.30; N, 7.19. ^{1}H NMR (500MHz, $CDCl_3$): ^{1}H NMR (500 MHz, $CDCl_3$) δ 1.48 (t, J = 9.4 Hz, 6H, CH_3), 4.12 (q, J = 7.0 Hz, 4H, OCH_2), 4.46 (s, 4H, CH_2), 6.83 (t, J = 3.1 Hz, 4H, ArH), 6.91 (dd, J = 4.9, 2.4 Hz, 2H, ArH), 8.26 (s, 2H, CH=N), 9.69 (s, 2H, OH).

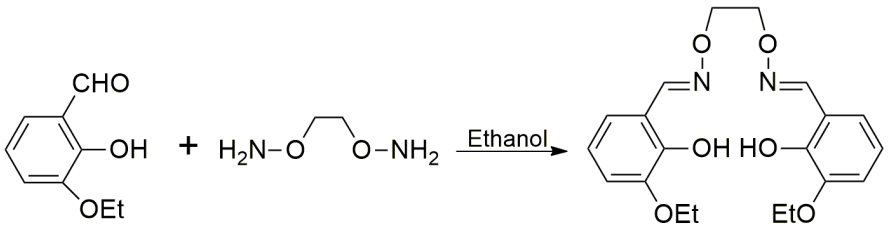

Scheme 1. Synthetic route to the salamo-like ligand H_2L.

2.3. Preparation of the Coordination Polymer

A solution of gadolinium nitrate hexahydrate (27.5 mg, 0.05 mmol) and nickel acetate tetrahydrate (12.4 mg, 0.05 mmol) in ethanol (5.0 mL) were added dropwise to a solution (5.0 mL) of H_2L in ethanol (5.0 mL), then a solution (5.0 mL) of terephthalic acid (16.6 mg, 0.1 mmol) in DMF was added to the

mixed solution. The mixture color changed to green immediately, and the mixture was kept stirring for 1 h. Then the mixture was filtered and the filtrate was obtained. The crystals suitable for X-ray crystallographic analysis were obtained by vapor diffusion of diethyl ether into the resulting filtrate for a few weeks at room temperature. Yield: 54.8%. Anal. Calcd for $_{\infty}$[(L)Ni(BDC)Gd(NO_3)(DMF)] ($C_{31}H_{33}GdN_4NiO_{14}$) (%): C, 41.31; H, 3.69; N, 6,21; Gd, 17.44, Ni, 6.51. Found: C, 41.48; H, 3.54; N, 6.12; Gd, 17.01, Ni, 6.10.

2.4. X-ray Crystallography

The single crystal of the polymer was collected by a SuperNova Dual Eos four-circle diffractometer, monochromatic Mo-Kα radiation (λ = 0.71073 Å) was carried out with a graphite monochromator and then processed with Olex2-2009. The crystal structure was solved with ShelXT-2015 and refined with ShelXL-2015 [62]. The anisotropic thermal parameters are assigned to all non–hydrogen atoms. CCDC 1957944. The crystallographic data for the Ni^{II}-Gd^{III} coordination polymer was listed in Table 1.

Table 1. Crystallographic data for the Ni^{II}-Gd^{III} coordination polymer.

Compond	The Ni^{II}-Gd^{III} Coordination Complex
Formula	$C_{31}H_{33}GdN_4NiO_{14}$
Formula weight	901.57
Temperature (K)	100.00(10)
Radiation (Å)	0.71073
Crystal system	monoclinic
Space group	$P\ 2_1/n$
a (Å)	10.8324 (7)
b (Å)	18.4853 (11)
c (Å)	17.7452 (12)
α (°)	90
β (°)	104.790 (7)
γ (°)	90
V (Å^3)	3435.6 (4)
Z	4
D_c (g·cm^{-3})	1.743
μ (mm^{-1})	2.536
F (000)	1804
Crystal size (mm)	0.11 × 0.09 × 0.08
θ Range (°)	2.203–29.566
Index ranges	−14 ≤ h ≤ 11 −23 ≤ k ≤ 23 −22 ≤ l ≤ 19
Completeness to θ	*84.3%* (θ = 25.242)
Tot. Date	18,620
Uniq. Date	8118
R (int)	0.0397
Observed Date	6605
Nref/Npar	8118/464
GOF	1.020
R[I/>2σ(I)]	R_1 = 0.0396, R_2 = 0.0846
Largest diff. peak and hole (e·Å^{-3})	−0.88, 1.45

$R_1 = \Sigma||F_o| - |F_c||/\Sigma|F_o|$; $\omega R_2 = [\Sigma\omega(F_o^2 - F_c^2)^2/\Sigma\omega(F_o^2)^2]^{1/2}$; GOF = $[\Sigma\omega(F_o^2 - F_c^2)^2/n_{obs} - n_{param})]^{1/2}$.

3. Results and Discussion

3.1. Solubility and Molar Conductance

The Ni^{II}-Gd^{III} polymer can be soluble in DMF and DMSO, slightly soluble in acetone, methanol, ethanol, trichloromethane, dichloromethane, and acetonitrile, and insoluble in ethyl ether, n-hexane, ethyl acetate, and water. The molar conductance of the Ni^{II}-Gd^{III} polymer dissolved in DMF at 25 °C (1×10^{-3} mol L^{-1}) is 174.2 $\Omega^{-1}\cdot cm^2\cdot mol^{-1}$. The molar conductivity result is close to the previously reported 1:2 electrolyte [63]. The Ni^{II}-Gd^{III} polymer dissolved in DMF may be comprised of $[Gd(DMF)_2]^{3+}$ cation and $[(L)Ni(BDC)]^{2-}$ and NO_3^- anions. The observed conductance would then correspond to the following equilibria taking place in solution:

$$[(L)Ni(BDC)Gd(NO_3)(DMF)] \rightleftharpoons [(L)Ni(BDC)]^{2-} + [Gd(NO_3)(DMF)]^{2+}$$

$$[Gd(NO_3)(DMF)]^{2+} + DMF \rightleftharpoons [Gd(DMF)_2]^{3+} + NO_3^-$$

3.2. PXRD Analysis

A PXRD experiment was performed for the Ni^{II}-Gd^{III} coordination polymer to confirm whether the crystal structure is truly representative. The PXRD pattern of the Ni^{II}-Gd^{III} coordination polymer is depicted in Figure 1. The experimental pattern is in good agreement with the simulated one through detailed comparison. Thus, the as-synthesized sample is pure enough for the further research of spectral characterization and fluorescence property.

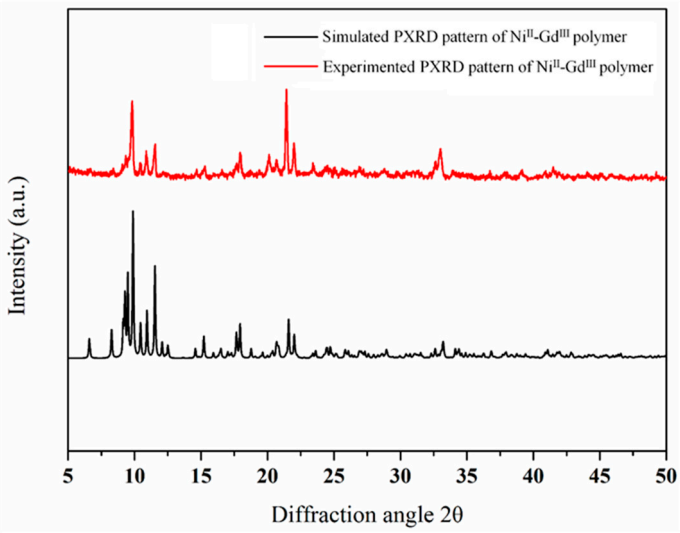

Figure 1. Comparing the simulated PXRD (black) and experimental patterns of the Ni^{II}-Gd^{III} coordination polymer.

3.3. FT-IR Spectra

The infrared spectra of H_2L and its Ni^{II}-Gd^{III} coordination polymer are given in Figure 2. The C=N stretching vibration band of H_2L is observed at *ca.* 1611 cm^{-1}, while that of the Ni^{II}-Gd^{III} coordination polymer is found at *ca.* 1627 cm^{-1}. The O–H stretching band of H_2L is found at *ca.* 3452 cm^{-1} that belongs to the phenolic hydroxyl groups. Furthermore, the typical Ar–O stretching band of H_2L emerges at approximately 1248 cm^{-1}, and after coordination, the stretching band shifted to a low wave number emerges at approximately 1216 cm^{-1} [17,24]. In the coordination polymer, there is an unsymmetrical ν_{asCOO^-} stretching vibration band (1549 cm^{-1}) and a symmetric ν_{sCOO^-} stretching band (1496 cm^{-1}) of the terephthalic acid, indicating that the carboxylate is a bridge-shaped structure.

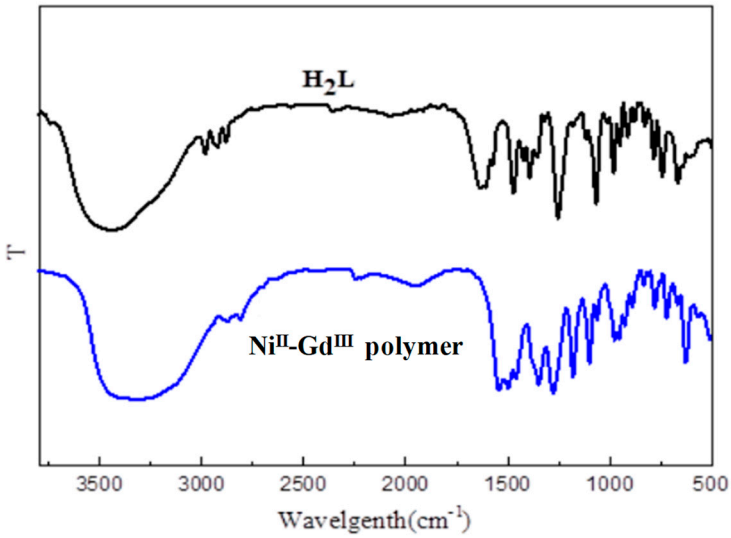

Figure 2. IR spectra of H_2L and its Ni^{II}-Gd^{III} coordination polymer.

3.4. UV-Vis Spectra

The free ligand H_2L and its Ni^{II}-Gd^{III} coordination polymer were dissolved and made into 1×10^{-5} M methanol solution, and their UV-Vis absorption spectra are depicted in Figure 3. It can be seen that their UV-Vis absorption spectra are obviously different. The UV-Vis absorption spectrum of H_2L possesses two strong absorption peaks at about 270 and 318 nm. The peak at 270 nm could be part of the π–π^* transition of the benzene rings, and the peak at 318 nm can be part of the intra-ligand π–π^* transition of the C=N bonds [11,37]. Compared with the peaks of H_2L, a new absorption peak is found at about 320 nm upon coordination, which is part of the n–π^* transition from the filled pπ orbital of the bridging phenolic O to the vacant d-orbital of the Ni^{II} ions [28,29].

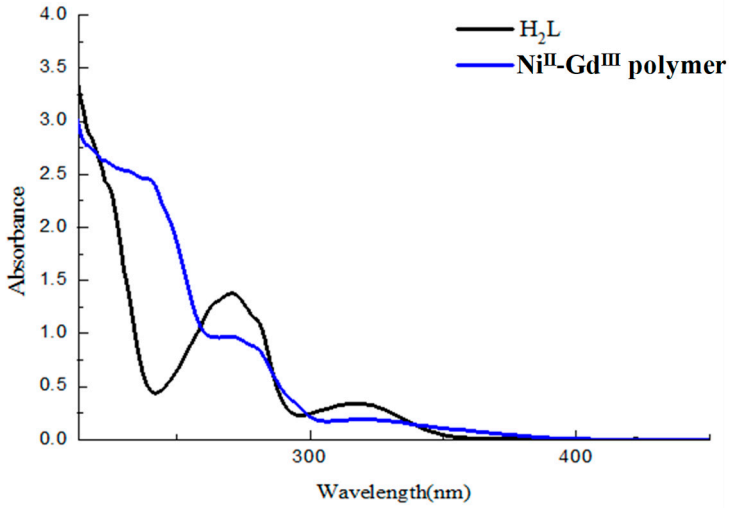

Figure 3. The UV-visible absorption spectra of H_2L and its Ni^{II}-Gd^{III} coordination polymer dissolved in methanol.

3.5. Crystal Structure Description

The molecule structure of the Ni^{II}-Gd^{III} coordination polymer and coordination geometries of metal(II/III) ions are depicted in Figure 4, and the essential bond lengths and angles are summarized in Table 2. The X-ray crystallographic result reveals that the Ni^{II}-Gd^{III} coordination polymer crystallizes in the monoclinic system, space group $P\ 2_1/n$, an asymmetric unit of the coordination polymer contains

one wholly deprotonated L^{2-} unit, one Ni^{II} ion (Ni1), one Gd^{III} ion (Gd1), one nitrate group, one DMF, and one terephthalic acid molecule.

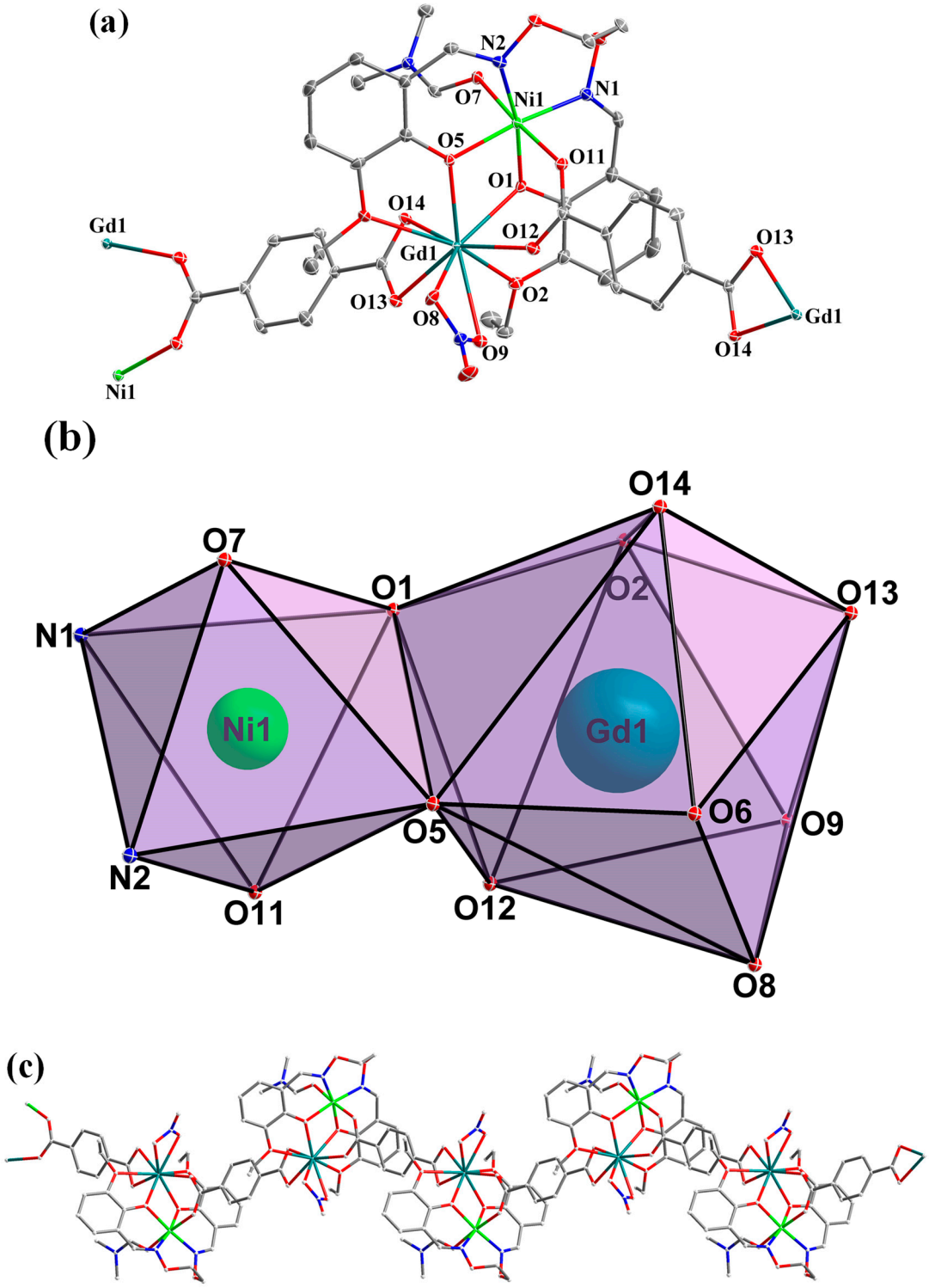

Figure 4. (**a**) Molecule structure and atom numberings of the Ni^{II}-Gd^{III} coordination polymer with 30% probability displacement ellipsoids; (**b**) coordination polyhedra for Ni^{II} and Gd^{III} ions of the coordination polymer; (**c**) view of 1-D chain structure of the Ni^{II}-Gd^{III} coordination polymer.

Table 2. Essential bond lengths (Å) and angles (°) for the Ni^{II}-Gd^{III} coordination polymer.

Bond	Dist.	Bond	Dist.	Bond	Dist.
Gd1–O1	2.378(2)	Gd1–O13 $^{\#1}$	2.416(3)	Ni1–N1	2.063(3)
Gd1–O2	2.521(3)	Gd1–O14 $^{\#1}$	2.482(3)	Ni1–N2	2.060(3)
Gd1–O5	2.336(3)	Ni1–O1	2.019(3)	Ni1–O7	2.091(3)
Gd1–O6	2.599(3)	Ni1–O5	2.025(2)	Ni1–O11	2.063(3)
Gd1–O8	2.473(3)	Gd1–O9	2.520(3)		
Bond	**Angles**	**Bond**	**Angles**	**Bond**	**Angles**
O1–Gd1–O2	63.76(9)	O2–Gd1–O6	149.31(10)	O5–Gd1–O12	82.51(9)
O1–Gd1–O5	68.34(8)	O2–Gd1–O8	122.89(10)	O5–Gd1–O13 $^{\#1}$	131.02(9)
O1–Gd1–O6	123.24(8)	O2–Gd1–O9	71.92(9)	O5–Gd1–O14 $^{\#1}$	90.05(9)
O1–Gd1–O8	145.56(10)	O2–Gd1–O12	87.78(10)	O5–Gd1–C31 $^{\#1}$	110.41(10)
O1–Gd1–O9	122.76(9)	O1–Gd1–O13 $^{\#1}$	78.28(10)	O7–Ni1–N2	86.07(12)
O1–Gd1–O12	73.76(9)	O1–Gd1–O14 $^{\#1}$	80.07(10)	O6–Gd1–O8	70.28(10)
O1–Gd1–O13 $^{\#1}$	126.03(9)	O1–Gd1–C31 $^{\#1}$	79.59(11)	O6–Gd1–O9	113.51(9)
O1–Gd1–O14 $^{\#1}$	81.99(9)	O5–Gd1–O6	62.21(8)	O6–Gd1–O12	122.81(10)
O1–Gd1–C31 $^{\#1}$	105.41(10)	O5–Gd1–O8	98.84(9)	O6–Gd1–O13 $^{\#1}$	74.78(10)
O2–Gd1–O5	131.95(9)	O5–Gd1–O9	143.56(9)	O6–Gd1–O14 $^{\#1}$	72.24(10)
O6–Gd1–C31 $^{\#1}$	69.72(11)	O9–Gd1–O13 $^{\#1}$	73.97(10)	O13$^{\#1}$–Gd1–31 $^{\#1}$	26.98(10)
O8–Gd1–O9	51.00(10)	O9–Gd1–O14 $^{\#1}$	124.44(9)	O14$^{\#1}$–Gd1–31 $^{\#1}$	26.72(10)
O8–Gd1–O12	72.90(10)	O9–Gd1–C31 $^{\#1}$	100.01(10)	O1–Ni1–O5	81.82(10)
O8–Gd1–O13 $^{\#1}$	86.97(10)	O12–Gd1–O13 $^{\#1}$	143.91(10)	O1–Ni1–O7	91.33(10)
O8–Gd1–O14 $^{\#1}$	131.28(10)	O12–Gd1–O14 $^{\#1}$	155.71(10)	O1–Ni1–O11	90.02(11)
O8–Gd1–C31 $^{\#1}$	109.03(11)	O12–Gd1–C31 $^{\#1}$	166.02(11)	O1–Ni1–N1	89.95(12)
O9–Gd1–O12	70.06(10)	O13$^{\#1}$–Gd1–14 $^{\#1}$	53.60(9)	O1–Ni1–N2	169.75(12)
O5–Ni1–O7	92.62(10)	O7–Ni1–O11	175.67(11)	O11–Ni1–N2	93.31(12)
O5–Ni1–O11	91.64(11)	O7–Ni1–N1	87.35(12)	N1–Ni1–N2	99.83(13)
O5–Ni1–N1	171.76(12)	O7–Ni1–N2	86.07(12)	Gd1 $^{\#2}$–C31–O14	62.0(2)
O5–Ni1–N2	88.39(12)	O11–Ni1–N1	88.54(13)	Gd1 $^{\#2}$–C31–C28	171.4(3)
Gd1 $^{\#2}$–C31–O13	59.03(19)	Gd1 $^{\#2}$–O13–C31	94.0(2)	Gd1 $^{\#2}$–O13–C31	91.3(2)

Symmetry transformations used to generate equivalent atoms: $^{\#1}$ x + 1/2, −y + 1/2, z − 1/2, $^{\#2}$ x − 1/2, −y + 1/2, z + 1/2.

The six-coordinated Ni1 ion lies at the N_2O_2 donor site of the ligand L^{2-} unit, and one DMF O atom and carboxylate O atom occupy, collectively, the axial positions, and form a twisted octahedron. The nine-coordinated Gd1 ion consists of three O atoms (O12, O13, and O14) of two carboxylate molecules, two O atoms (O8 and O9) derived from one bidentate nitrate group, and an O_2O_2 coordination site (O1, O2, O6, and O5) of the ligand L^{2-} unit, forming a twisted three-capped triangular prism coordination geometry. The salamo-like ligand H_2L can be self-assembled with some bridging ligands and metal salts to obtain multiple complexes or polymers due to its structural specificity [64]; here, terephthalic acid, as a tetradentate connecting agent, can connect Ni^{II} and Gd^{III} ions to form a chain coordination polymer.

Furthermore, the hydrogen bonding interactions of the Ni^{II}-Gd^{III} coordination polymer are listed in Table 3. In the structure of the Ni^{II}-Gd^{III} coordination polymer, there are seven intra-molecular hydrogen bonding interactions (C7–H7B···O13, C11–H11B···O11, C19–H19B···O13, C20–H20C···O8, C21–H21···O5, C23–H23A···O7, and C27–H27···O13) [65–73] (Figure 5a) and four inter-molecular hydrogen bonding interactions (C9–H9...O10, C10–H10A...O9, C19–H19B...O5, and C20–H20B...O3) (Figure 5b), and an infinite 1-D chain supramolecular structure is formed by inter-molecular hydrogen bonding interactions.

Table 3. Hydrogen bond parameters (Å, °) for the Ni^{II}-Gd^{III} coordination polymer.

D–H···A	d(D–H)	d(H···A)	d(D···A)	∠D–H···A	Symmetry Code
C7–H7B···O13	0.97	2.55	3.163(5)	121	–1/2 + x, 1/2–y, 2 + z
C9–H9···O10	0.93	2.56	3.456(5)	163	3/2 − x, 1/2+ y, 3/2 − z
C10–H10A···O9	0.97	2.54	3.259(6)	131	3/2 − x, 1/2+y, 3/2 − z
C11–H11B···O11	0.97	2.24	3.169(5)	159	
C19–H19B···O4	0.97	2.50	3.105(5)	120	1/2 − x, −1/2 + y,3/2 − z
C19–H19B··O13	0.97	2.47	3.146(6)	128	–1/2 + x, 1/2 − y, 2 + z
C20–H20B···O3	0.96	2.49	3.396(6)	157	1/2 − x, 1/2 + y, 3/2 − z
C20–H20C···O8	0.96	2.41	3.185(6)	138	
C21–H21···O5	0.93	2.56	3.090(4)	116	
C21–H21···O14	0.93	2.46	2.258(5)	148	–1/2 + x, 1/2 − y, 2 + z
C23–H23A···O7	0.96	2.44	2.810(5)	103	
C23–H27···O13	0.96	2.49	2.796(5)	100	

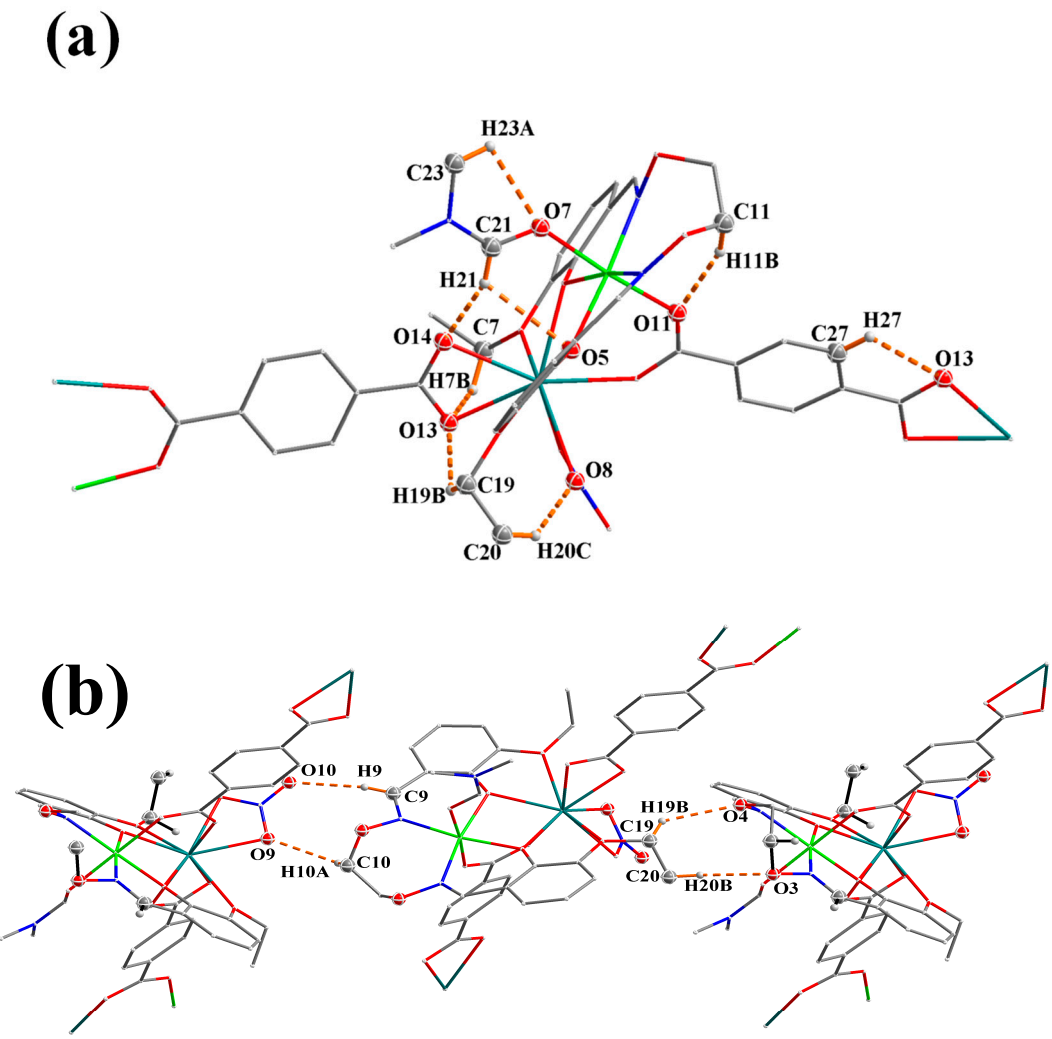

Figure 5. View of the intramolecular (**a**) and intermolecular (**b**) hydrogen bonding interactions of the Ni^{II}-Gd^{III} coordination polymer.

3.6. Fluorescence Properties

Photophysical properties of lanthanide complexes of salen-like and salamo-like ligands have been successfully reported previously [74]. The free ligand H_2L and its Ni^{II}-Gd^{III} coordination polymer were dissolved and made into a 2.5×10^{-5} M methanol solution, and their fluorescence spectra excited

at 315 nm are revealed in Figure 6. H_2L has the strongest absorption peak at about 404 nm, probably owing to the π–π* transition of the L^{2-} unit. Compared to the free ligand H_2L, a stronger emission peak at approximately 404 nm is observed upon coordination, which is attributable to the coordination of the L^{2-} unit and metal ions; the conjugated system upon coordination decreases.

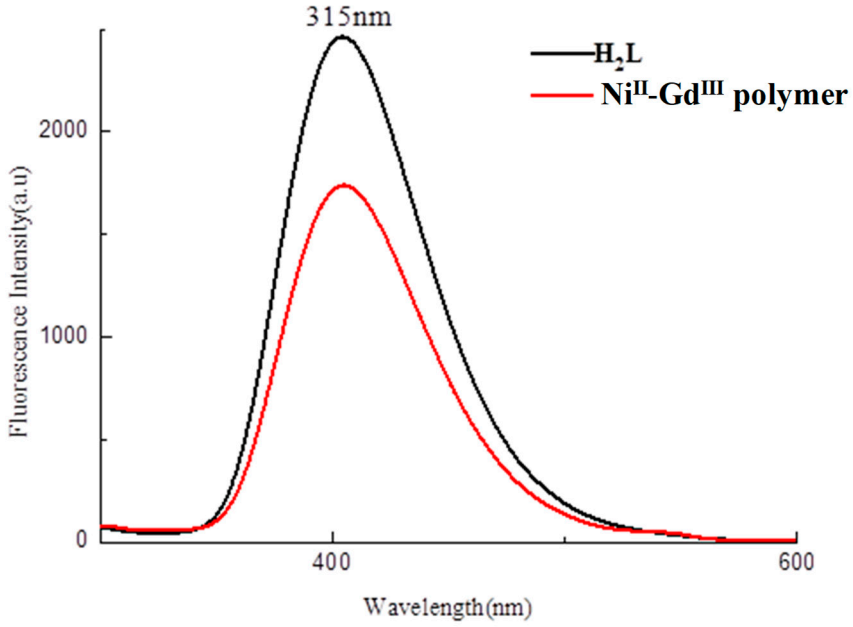

Figure 6. Emission spectra of H_2L and its Ni^{II}-Gd^{III} coordination polymer dissolved in CH_3OH.

3.7. DFT Calculation

In order to understand the electronic structure and properties of the polymer, a DFT calculation was performed on the polymer using Gaussian 09 [75] (Figure 7). The graph of the highest occupied molecular orbitals (HOMOs) of the polymer indicates that the HOMOs are delocalized, mainly in the orbit of Ni^{II}-Gd^{III} ions. LUMOs are relatively limited to the auxiliary ligands of terephthalic acid and Ni^{II}-Gd^{III} orbitals. The frontier molecular orbital energy of the polymer is E_{HOMO} = −4.4792 eV and E_{LUMO} = −2.3518 eV. The polymer HOMO–LUMO gap is 2.12177 eV. The molecular orbital energy occupied by the polymer is all negative, indicating molecular chemical stability. The polymer has a lower HOMO–LUMO energy gap ($\Delta E = E_{LUMO} - E_{HOMO}$), and the smaller the ΔE value, the more active the molecule.

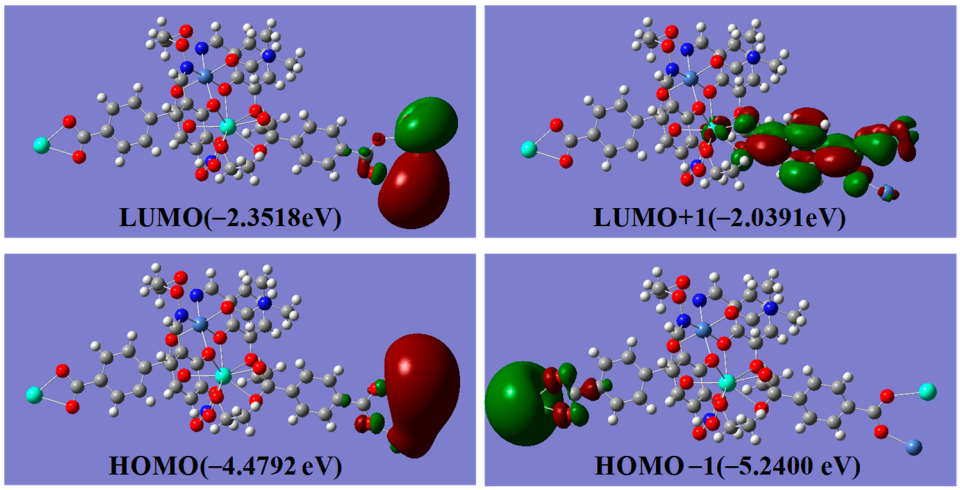

Figure 7. Molecular orbital map of DFT calculation of the Ni^{II}-Gd^{III} polymer.

3.8. Antibacterial Activities

This paper chooses DMF as the solvent and configured the ligand, nickel acetate, cerium nitrate, the Ni^{II}-Gd^{III} polymer, and ampicillin as solutions to be tested. Four sets of different concentrations of DMF solutions were prepared–0.4, 0.8, 1.6, and 3.2 mg/mL. For ease of analysis, we distributed the bacterial inoculant evenly over a flat surface, placing the impregnated plate near the edge of the flat surface and maintaining a certain distance. Ampicillin was used as a positive experiment under the same condition and 200 µL sample was put into LB solid medium, and all samples were incubated at 32 °C for 12 h.

The ampicillin inhibition zone diameter was the best in various samples at a concentration of 3.2 mg/mL. As depicted in Figure 8, the inhibitory regions of DMF, nickel(II) acetate, gadolinium nitrate, H_2L, ampicillin, and the coordination polymer dissolved in DMF gradually increased, and show that the coordination polymer dissolved in DMF has a good antibacterial activity. Firstly, due to the heavy metal ion effect force in the polymer, protein structure in the bacteria are destroyed. Secondly, the ligand also destroys part of the bacterial membrane, and the bacteria cannot further divide and multiply and thus die. These observations are similar to the biological activities of previously successfully reported complexes [76–79].

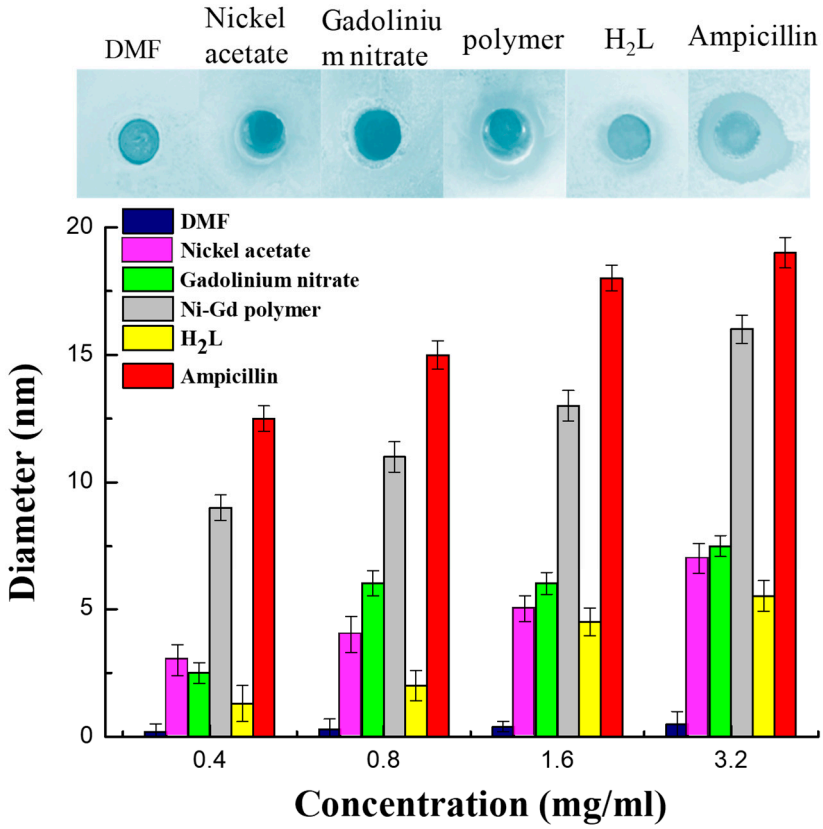

Figure 8. The inhibition zones diameter of ampicillin in various concentrations of different samples.

4. Conclusions

An unprecedented hetero-bimetallic 3d-4f coordination polymer, [(L)Ni(BDC)Gd(NO_3)(DMF)] was designed and synthesized, and the single crystal structure was validated via X-ray crystallography. The coordination polymer forms a 1-D supra-molecular chain structure, and the nine-coordinated Gd^{III} ion is located in an O_9 coordination environment and forms a twisted three-capped triangular prism coordination geometry. The six-coordinated Ni1 ion lies at the N_2O_2 donor site of the L^{2-} unit, and one DMF O atom and carboxylate O atom occupy, collectively, the axial positions, and form a twisted octahedron. In addition, the polymer dissolved in DMF has good antibacterial activity due to

the heavy metal ion effect of the Ni^{II}-Gd^{III} coordination polymer, and a stronger emission peak appears at about 404 nm. The structure of the polymer was rationalized by DFT calculation. In addition, the possible form of the polymer dissolved in DMF was investigated by measuring the molar conductivity.

Author Contributions: W.-K.D. conceived and designed the experiments; Y.-F.C. and Y.Z. performed the experiments; Y.Z. analyzed the data; K.-F.X., formal analysis; W.-K.D. contributed reagents/materials/analysis tools; W.-K.D. and Y.-F.C. wrote the paper.

Funding: This research was funded by the National Natural Science Foundation of China (Grant No. 21761018), the Science and Technology Program of Gansu Province (Grant No. 18YF1GA057) and the Program for Excellent Team of Scientific Research in Lanzhou Jiaotong University (Grant No. 201706.

Acknowledgments: Computations were done using National Supercomputing Center in Shenzhen, P. R. China.

Conflicts of Interest: The authors declare no competing financial interests.

References

1. Akine, S.; Varadi, Z.; Nabeshima, T. Synthesis of planar metal complexes and the stacking abilities of naphthaenediol-based acyclic and macrocyclic salen-type ligands. *Eur. J. Inorg. Chem.* **2013**, *35*, 5987–5998. [CrossRef]
2. Kang, Q.P.; Li, X.Y.; Wei, Z.L.; Zhang, Y.; Dong, W.K. Symmetric containing-PMBP N_2O_2-donors nickel (II) complexes: Syntheses, structures, Hirshfeld analyses and fluorescent properties. *Polyhedron* **2019**, *165*, 38–50. [CrossRef]
3. Wu, H.L.; Bai, Y.C.; Zhang, Y.H.; Pan, G.L.; Kong, J.; Shi, F.; Wang, X.L. Two lanthanide (III) complexes based on the schiff base *N*, *N*-Bis (salicylidene)-1,5-diamino-3-oxapentane: Synthesis, characterization, DNA-binding properties, and antioxidation. *Z. Anorg. Allg. Chem.* **2014**, *640*, 2062–2071. [CrossRef]
4. Kang, Q.P.; Li, X.Y.; Wang, L.; Zhang, Y.; Dong, W.K. Containing-PMBP N_2O_2-donors transition metal (II) complexes: Synthesis, crystal structure, Hirshfeld surface analyses and fluorescence properties. *Appl. Organomet. Chem.* **2019**, *33*, e5013. [CrossRef]
5. Wu, H.L.; Bai, Y.C.; Zhang, Y.H.; Li, Z.; Wu, M.C.; Chen, C.Y.; Zhang, J.W. Synthesis, crystal structure, antioxidation and DNA-binding properties of a dinuclear copper (II) complex with bis (N-salicylidene)-3-oxapentane-1, 5-diamine. *J. Coord. Chem.* **2014**, *67*, 3054–3066. [CrossRef]
6. Gao, L.; Wang, F.; Zhao, Q.; Zhang, Y.; Dong, W.K. Mononuclear Zn(II) and trinuclear Ni(II) complexes derived from a coumarin-containing N_2O_2 ligand: Syntheses, crystal structures and fluorescence properties. *Polyhedron* **2018**, *139*, 7–16. [CrossRef]
7. Liu, Y.A.; Wang, C.Y.; Zhang, M.; Song, X.Q. Structures and magnetic properties of cyclic heterometallic tetranuclear clusters. *Polyhedron* **2017**, *127*, 278–286. [CrossRef]
8. Liu, P.P.; Sheng, L.; Song, X.Q.; Xu, W.Y.; Liu, Y.A. Synthesis, structure and magnetic properties of a new one dimensional manganese coordination polymer constructed by a new asymmetrical ligand. *Inorg. Chim. Acta* **2015**, *434*, 252–257. [CrossRef]
9. Song, X.Q.; Cheng, G.Q.; Liu, Y.A. Enhanced Tb (III) luminescence by d ^{10} transition metal coordination. *Inorg. Chim. Acta* **2016**, *450*, 386–394. [CrossRef]
10. Wang, P.; Zhao, L. An infinite 2D supramolecular cobalt (II) complex based on an asymmetric salamo-type ligand: Synthesis, crystal structure, and spectral properties. *Synth. React. Inorg. Met. -Org. Nano-Met. Chem.* **2016**, *46*, 1095–1101. [CrossRef]
11. Zhang, Y.; Liu, L.Z.; Peng, Y.D.; Li, N.; Dong, W.K. Structurally characterized trinuclear nickel (II) and copper (II) salamo-type complexes: Syntheses, Hirshfeld analyses and fluorescent properties Transit. *Met. Chem.* **2019**, *44*, 627–639. [CrossRef]
12. Sun, Y.X.; Zhang, S.T.; Ren, Z.L.; Dong, X.Y.; Wang, L. Synthesis, characterization, and crystal structure of a new supramolecular Cd^{II} complex with halogen-substituted salen-type bisoxime. *Synth. React. Inorg. Met.-Org. Nano-Met. Chem.* **2013**, *43*, 995–1000. [CrossRef]
13. Chattopadhyay, S.; Drew, M.G.B.; Ghosh, A. Methylene spacer-regulated structural variation in cobalt(II/III) complexes with bridging acetate and salen- or salpn-type Schiff-base ligands. *Eur. J. Inorg. Chem.* **2008**, *10*, 1693–1701. [CrossRef]

14. Liu, L.Z.; Wang, L.; Yu, M.; Zhao, Q.; Zhang, Y.; Sun, Y.X.; Dong, W.K. A highly sensitive and selective fluorescent "off-on-off" relay chemosensor based on a new bis (salamo)-type tetraoxime for detecting Zn^{2+} and CN^{-}. *Spectrochim. Acta A* **2019**, *222*, 7209. [CrossRef] [PubMed]
15. Song, X.Q.; Peng, Y.J.; Chen, G.Q.; Wang, X.R.; Liu, P.P.; Xu, W.Y. Substituted group-directed assembly of Zn (II) coordination complexes based on two new structural related pyrazolone based salen ligands: Syntheses, structures and fluorescence properties. *Inorg. Chim. Acta* **2015**, *427*, 13–21. [CrossRef]
16. Varga, Z.; Meana-Pañeda, R.; Song, G.L.; Paukku, Y.; Truhlar, D.G. Potential energy surface of triplet N_2O_2. *J. Chem. Phys.* **2016**, *144*, 8. [CrossRef]
17. Zhao, Q.; An, X.X.; Liu, L.Z.; Dong, W.K. Syntheses, luminescences and Hirshfeld surfaces analyses of structurally characterized homo-trinuclear Zn^{II} and hetero-pentanuclear Zn^{II}-Ln^{III} (Ln = Eu, Nd) bis(salamo)-like complexes. *Inorg. Chim. Acta* **2019**, *490*, 6–15. [CrossRef]
18. Akine, S.; Utsuno, F.; Taniguchi, T.; Nabeshima, T. Dinuclear complexes of the N_2O_2 oxime chelate ligand with zinc(II)-lanthanide(III) as a selective sensitization system for Sm^{3+}. *Eur. J. Inorg. Chem.* **2010**, *20*, 3143–3152. [CrossRef]
19. Łępicka, K.; Pieta, P.; Francius, G.; Walcarius, A.; Kutner, W. Structure-reactivity requirements with respect to nickel-salen based polymers for enhanced electrochemical stability. *Electrochim. Acta* **2019**, *315*, 75–83. [CrossRef]
20. Liu, X.; Manzurc, C.; Novoa, N.; Celedónc, S.; Carrilloc, D.; Hamon, J.R. Multidentate unsymmetrically substituted Schiff bases and their metal complexes: Synthesis, functional materials properties, and applications to catalysis. *Coord. Chem. Rev.* **2018**, *357*, 144–172. [CrossRef]
21. Finelli, A.; Hérault, N.; Crochet, A.; Fromm, K.M. Threading salen-type Cu- and Ni-complexes into one-dimensional coordination polymers: Solution versus solid state, and the size effect of the alkali metal ion. *Cryst. Growth Des.* **2018**, *18*, 1215–1226. [CrossRef]
22. Celedón, S.; Dorcet, V.; Roisnel, T.; Singh, A.; Ledoux-Rak, I.; Hamon, J.R.; Carrillo, D.; Manzur, C. Main-chain oligomers from Ni^{II}- and Cu^{II}-centered unsymmetrical N_2O_2 Schiff-base complexes: Synthesis and spectral, structural, and second-order nonlinear optical properties. *Eur. J. Inorg. Chem.* **2014**, *29*, 4984–4993.
23. Akine, S. Novel ion recognition systems based on cyclic and acyclic oligo (salen)-type ligands. *J. Incl. Phenom. Macrocycl. Chem.* **2012**, *72*, 25–54. [CrossRef]
24. Li, X.Y.; Chen, L.; Gao, L.; Zhang, Y.; Akogun, S.F.; Dong, W.K. Syntheses, crystal structures and catalytic activities of two solvent-induced homotrinuclear Co (II) complexes with a naphthalenediol-based bis(Salamo)-type tetraoxime ligand. *RSC Adv.* **2017**, *7*, 35905–35916. [CrossRef]
25. Li, X.Y.; Kang, Q.P.; Liu, C.; Zhang, Y.; Dong, W.K. Structurally characterized homo-trinuclear Zn^{II} and hetero-pentanuclear [$Zn^{II}_4Ln^{III}$] complexes constructed from an octadentate bis(Salamo)-based ligand: Hirshfeld surfaces, fluorescence and catalytic properties. *New J. Chem.* **2019**, *43*, 4605–4619. [CrossRef]
26. Wu, H.L.; Pan, G.L.; Bai, Y.C.; Zhang, Y.H.; Wang, H.; Shi, F.R.; Wang, X.L.; Kong, J. Study on synthesis, crystal structure, antioxidant and DNA-binding of mono-, di- and poly-nuclear lanthanides complexes with bis (N-salicylidene)-3-oxapentane-1,5-diamine. *J. Photochem. Photobiol. B* **2014**, *135*, 33–43. [CrossRef]
27. Wu, H.L.; Pan, G.L.; Bai, Y.C.; Wang, H.; Kong, J.; Shi, F.R.; Zhang, Y.H.; Wang, X.L. Preparation, structure, DNA-binding properties, and antioxidant activities of a homodinuclear erbium (III) complex with a pentadentate Schiff base ligand. *J. Chem. Res.* **2014**, *38*, 211–217. [CrossRef]
28. Wu, H.L.; Wang, C.P.; Wang, F.; Peng, H.P.; Zhang, H.; Bai, Y.C. A new manganese (III) complex from bis(5-methylsalicylaldehyde)-3-oxapentane-1,5-diamine: Synthesis, characterization, antioxidant activity and luminescence. *J. Chin. Chem. Soc.* **2015**, *62*, 1028–1034. [CrossRef]
29. Song, X.Q.; Liu, P.P.; Liu, Y.A.; Zhou, J.J.; Wang, X.L. Two dodecanuclear heterometallic [Zn_6Ln_6] clusters constructed by a multidentate salicylamide salen-like ligand: Synthesis, structure, luminescence and magnetic properties. *Dalton Trans.* **2016**, *45*, 8154–8163. [CrossRef]
30. Li, J.; Zhang, H.J.; Chang, J.; Jia, H.R.; Sun, Y.X.; Huang, Y.Q. Solvent-induced unsymmetric salamo-like trinuclear Ni^{II} complexes: Syntheses, crystal structures, fluorescent and magnetic properties. *Crystals* **2018**, *8*, 176. [CrossRef]
31. Liu, P.P.; Wang, C.Y.; Zhang, M.; Song, X.Q. Pentanuclear sandwich-type Zn^{II}-Ln^{III} clusters based on a new Salen-like salicylamide ligand: Structure, near-infrared emission and magnetic properties. *Polyhedron* **2017**, *129*, 133–140. [CrossRef]

32. Petrick, M.; Florian, B.; Katja, L.; Guntram, R.; Réne, P. Cooperative Al(Salen)-pyridinium catalysts for the asymmetric synthesis of trans-configured β-Lactones by [2+2]-cyclocondensation of acylbromides and aldehydes: Investigation of pyridinium substituent effects. *Molecule* **2012**, *17*, 7121–7150.
33. Song, X.Q.; Liu, P.P.; Wang, C.Y.; Liu, Y.A.; Liu, W.S.; Zhang, M. Three sandwich-type zinc (II)-lanthanide (III) clusters: Structures, luminescence and magnetic properties. *RSC Adv.* **2017**, *7*, 22692–22698. [CrossRef]
34. Chai, L.Q.; Huang, J.J.; Zhang, H.S. An unexpected cobalt (III) complex containing a Schiff base ligand: Synthesis, crystal structure, spectroscopic behavior, electrochemical property and SOD-like activity. *Spectrochim. Acta A* **2014**, *131*, 526–530. [CrossRef] [PubMed]
35. Chai, L.Q.; Tang, L.J.; Chen, L.C.; Huang, J.J. Structural, spectral, electrochemical and DFT studies of two mononuclear manganese (II) and zinc (II) complexes. *Polyhedron* **2017**, *122*, 228–240. [CrossRef]
36. Chai, L.Q.; Huang, J.J.; Zhang, J.Y.; Li, Y.X. Two 1-D and 2-D cobalt (II) complexes: Synthesis, crystal structures, spectroscopic and electrochemical properties. *J. Coord. Chem.* **2015**, *68*, 1224–1237. [CrossRef]
37. Chai, L.Q.; Li, Y.X.; Chen, L.C.; Zhang, J.Y.; Huang, J.J. Synthesis, X-ray structure, spectroscopic, electrochemical properties and DFT calculation of a bridged dinuclear copper(II) complex. *Inorg. Chim. Acta* **2016**, *444*, 193–201. [CrossRef]
38. Bhowmik, P.; Nayek, H.P.; Corbella, M.; Aliaga-Alcalde, N.; Chattopadhyay, S. Control of molecular architecture by steric factors: Mononuclear vs polynuclear manganese (III) compounds with tetradentate N_2O_2 donor Schiff bases. *Dalton Trans.* **2011**, *40*, 7916–7926. [CrossRef]
39. Dong, W.K.; Ma, J.C.; Zhu, L.C.; Zhang, Y. Self-assembled zinc (II)-lanthanide (III) heteromultinuclear complexes constructed from 3-MeO salamo ligand: Syntheses, structures and luminescent properties. *Cryst. Growth Des.* **2016**, *16*, 6903–6914. [CrossRef]
40. Dong, X.Y.; Kang, Q.P.; Li, X.Y.; Ma, J.C.; Dong, W.K. Structurally characterized solvent-induced homotrinuclear cobalt (II) N_2O_2-donor bisoxime-type complexes. *Crystals* **2018**, *8*, 139. [CrossRef]
41. Novozhilova, M.V.; Smirnova, E.A.; Polozhentseva, J.A.; Danilova, J.A.; Chepurnaya, I.A.; Karushev, M.P.; Malev, V.V.; Timonov, A.M. Multielectron redox processes in polymeric cobalt complexes with N_2O_2 Schiff base ligands. *Electrochim. Acta* **2018**, *282*, 105–115. [CrossRef]
42. Zhao, L.; Dang, X.T.; Chen, Q.; Zhao, J.X.; Wang, L. Synthesis, crystal structure and spectral properties of a 2D supramolecular copper (II) complex with 1-(4-{[(E)-3-ethoxyl-2-hydroxybenzylidene]amino}phenyl)ethanone oxime. *Synth. React. Inorg. Met.-Org. Nano-Met. Chem.* **2013**, *43*, 1241–1246. [CrossRef]
43. Yamamura, M.; Takizawa, H.; Sakamoto, N.; Nabeshima, T. Monomeric and dimeric red/NIR-fluorescent dipyrrin-germanium complexes: Facile monomer-dimer interconversion driven by acid/base additions. *Tetrahedron Lett.* **2013**, *54*, 7049–7052. [CrossRef]
44. Manna, A.K.; Mondal, J.; Chandra, R.; Rout, K.; Patra, G.K. A fluorescent colorimetric azo dye based chemosensor for detection of S^{2-} in perfect aqueous solution and its applications in real sample analysis and molecular logic gate. *Sens. Actuators B* **2018**, *10*, 2317–2326. [CrossRef]
45. Zhou, L.; Cai, P.; Fen, Y.; Cheng, J.; Xiang, H.; Liu, J.; Wu, D.; Zhou, X. Synthesis and photophysical properties of water-soluble sulfonato-Salen-type Schiff bases and their applications of fluorescence sensors for Cu^{2+} in water and living cells. *Anal. Chim. Acta* **2012**, *735*, 96–106. [CrossRef] [PubMed]
46. Pushkarev, A.P.; Balashova, T.V.; Kukinov, A.A.; Arsenyev, M.V.; Yablonskiy, A.N.; Kryzhkov, D.I.; Andreev, B.A.; Rumyantcev, R.V.; Fukin, G.K.; Bochkarev, M.N. Sensitization of NIR luminescence of Yb^{3+} by Zn^{2+} chromophores in heterometallic complexes with a bridging Schiff-base ligand. *Dalton Trans.* **2017**, *46*, 10408–10417. [CrossRef] [PubMed]
47. Peng, Y.D.; Li, X.Y.; Kang, Q.P.; An, G.X.; Zhang, Y.; Dong, W.K. Synthesis and fluorescence properties of asymmetrical salamo-type tetranuclear zinc (II) complex. *Crystals* **2018**, *8*, 107. [CrossRef]
48. Peng, Y.D.; Wang, F.; Gao, L.; Dong, W.K. Structurally characterized dinuclear zinc (II) bis(salamo)-type tetraoxime complex possessing square pyramidal and trigonal bipyramidal geometries. *J. Chin. Chem. Soc.* **2018**, *65*, 893–899. [CrossRef]
49. Wang, F.; Liu, L.Z.; Gao, L.; Dong, W.K. Unusual constructions of two salamo-based copper (II) complexes. *Spectrochim. Acta A* **2018**, *203*, 56–64. [CrossRef]
50. Li, X.Y.; Kang, Q.P.; Liu, L.Z. Trinuclear Co (II) and mononuclear Ni (II) salamo-type bisoxime coordination compounds. *Crystals* **2018**, *8*, 43. [CrossRef]
51. Dong, X.Y.; Zhao, Q.; Wei, Z.L.; Mu, H.R.; Zhang, H.; Dong, W.K. Synthesis and fluorescence propertiesof structurally characterized heterobimetalic Cu (II)-Na (I) bis (salamo)-based complex bearing square planar,

square pyramid and triangular prism geometries of metal centers. *Molecules* **2018**, *23*, 1006. [CrossRef] [PubMed]
52. Gao, L.; Liu, C.; Wang, F.; Dong, W.K. Tetra-, penta- and hexa-coordinated transition metal complexes constructedfrom coumarin-containing N_2O_2 ligand. *Crystals* **2018**, *8*, 77. [CrossRef]
53. Wang, L.; Kang, Q.P.; Hao, J.; Dong, W.K. Two trinuclear cobalt(Il) salamo-type complexes: Syntheses, crystal structures, solvent effect and fluorescent properties. *Chin. J. Inorg. Chem.* **2018**, *34*, 525–533.
54. Kang, Q.P.; Li, X.Y.; Zhao, Q.; Ma, J.C.; Dong, W.K. Structurally characterized homotrinuclear Salamo-type nickel (lI) complexes: Synthesis, solvent effect and fluorescence properties. *Appl. Organomet. Chem.* **2018**, *32*, e4379. [CrossRef]
55. Hao, J.; Li, X.Y.; Zhang, Y.; Dong, W.K. A reversible bis(salamo)-based fluorescence sensor for selective detection of Cd^{2+} in water-containing systems and food samples. *Materials* **2018**, *11*, 523. [CrossRef]
56. Zhang, L.W.; Li, X.Y.; Kang, Q.P. Liu, L.Z. Ma, J.C. Dong, W.K. Structures and fluorescent and magnetic behaviors of newly synthesized Ni^{II} and Cu^{II} coordination compounds. *Crystals* **2018**, *8*, 173. [CrossRef]
57. Ren, Z.L.; Hao, J.; Hao, P.; Dong, X.Y.; Bai, Y.; Dong, W.K. Synthesis, crystal structure, luminescence and electrochemical properties of a salamo-type trinuclear cobalt (II) complex. *Z. Nat. B* **2018**, *73*, 203–210. [CrossRef]
58. Zhang, L.W.; Liu, L.Z.; Wang, F.; Dong, W.K. Unprecedented fluorescent dinuclear Co^{II} and Zn^{II} coordination compounds with a symmetric bis(salamo)-like tetraoxime. *Molecules* **2018**, *23*, 1141. [CrossRef]
59. Gulzhian, I.D.; Igor E, U. Design and synthesis of coordination polymers with chelated units and their application in nanomaterials science. *RSC Adv.* **2017**, *7*, 42242–42288.
60. Yang, Y.H.; Zhang, Y.; Yu, M.; Zheng, S.S.; Dong, W.K. Heterbimetallic Cu (II)-Nd (III) and Zn (II)-Ce (III) salamo-type complexes: Syntheses, crystal structure and fluorescence properties. *Chin. J. Inorg. Chem.* **2018**, *34*, 997–1006.
61. Akine, S.; Taniguchi, T.; Dong, W.K.; Masubuchi, S.; Nabeshima, T. Oxime-based salen-type tetradentate ligands with high stability against imine metathesis reaction. *J. Org. Chem.* **2005**, *70*, 1704–1711. [CrossRef] [PubMed]
62. Sheldrick, G.M. Acta Crystallogr. *Sect. C: Cryst. Struct. Commun.* **2015**, *71*, 3–8.
63. Geary, W.J. The use of conductivity measurements in organic solvents for the characterization of coordination compounds. *Coord. Chem. Rev.* **1971**, *7*, 81–122. [CrossRef]
64. Dong, W.K.; Ma, J.C.; Zhu, L.C.; Zhang, Y. Nine self–assembled nickel (II)-lanthanide (III) heterometallic complexes constructed from a salamo–type bisoxime and bearing N– or –donor auxiliary ligand: Syntheses, structures and magnetic properties. *New J. Chem.* **2016**, *40*, 6998–7010. [CrossRef]
65. Sun, Y.X.; Xu, L.; Zhao, T.H.; Liu, S.H.; Liu, G.H.; Dong, X.T. Synthesis and crystal structure of a 3D supramolecular copper (II) complex with 1-(3-{[(E)-3-bromo-5-chloro-2-hydroxybenzylidene]amino}phenyl) ethanone oxime. *Synth. React. Inorg. Met. -Org. Nano-Met. Chem.* **2013**, *43*, 509–513. [CrossRef]
66. An, X.X.; Zhao, Q.; Mu, H.R.; Dong, W.K. A new half-salamo-based homo-trinuclear nickel (II) complex: Crystal structure, Hirshfeld surface analysis, and fluorescence properties. *Crystals* **2019**, *9*, 101. [CrossRef]
67. Sun, Y.X.; Gao, X.H. Synthesis, characterization, and crystal structure of a new Cu^{II} complex with salen-type ligand. *Synth. React. Inorg. Met. -Org. Nano-Met. Chem.* **2011**, *41*, 973–978. [CrossRef]
68. Wang, P.; Zhao, L. Synthesis, structure and spectroscopic properties of the trinuclear cobalt (II) and nickel (II) complexes based on 2-hydroxynaphthaldehyde and bis (aminooxy)alkane. *Spectrochim. Acta A* **2015**, *135*, 342–350. [CrossRef]
69. Sun, Y.X.; Wang, L.; Dong, X.Y.; Ren, Z.L.; Meng, W.S. Synthesis, characterization, and crystal structure of a supramolecular Co^{II} complex containing salen-type bisoxime. *Synth. React. Inorg. Met.-Org. Nano-Met. Chem.* **2013**, *43*, 599–603. [CrossRef]
70. Chai, L.Q.; Liu, G.; Zhang, Y.L.; Huang, J.J.; Tong, J.F. Synthesis, crystal structure, fluorescence, electrochemical property, and SOD-like activity of an unexpected nickel (II) complex with a quinazoline-type ligand. *J. Coord. Chem.* **2013**, *66*, 3926–3938. [CrossRef]
71. Jia, H.R.; Chang, J.; Zhang, H.J.; Li, J.; Sun, Y.X. Three polyhydroxyl-bridged defective dicubane tetranuclear Mn^{III} complexes: Synthesis, crystal structures, and spectroscopic properties. *Crystals* **2018**, *8*, 272. [CrossRef]
72. Wu, H.L.; Bai, Y.; Yuan, J.K.; Wang, H.; Pan, G.L.; Fan, X.Y.; Kong, J. A zinc (II) complex with tris (2-(*N*-methyl) benzimidazlylmethyl) amine and salicylate: Synthesis, crystal structure, and DNA-binding. *J. Coord. Chem.* **2012**, *65*, 2839–2851. [CrossRef]

73. Wu, H.L.; Pan, G.L.; Bai, Y.C.; Wang, H.; Kong, J. Synthesis, structure, antioxidation, and DNA-bindingstudies of a binuclear ytterbium (III) complex with bis(N-salicylidene)-3-oxapentane-1,5-diamine. *Res. Chem. Intermed.* **2015**, *41*, 3375–3388. [CrossRef]
74. Zheng, S.S.; Dong, W.K.; Zhang, Y.; Chen, L.; Ding, Y.J. Four salamo-type 3d-4f hetero-bimetallic [$Zn^{II}Ln^{III}$] complexes: Syntheses, crystal structures, and luminescent and magnetic properties. *New J. Chem.* **2017**, *44*, 4966–4973. [CrossRef]
75. Chai, L.Q.; Hu, Q.; Zhang, K.Y.; Zhou, L.; Huang, J.J. Synthesis, structural characterization, spectroscopic, and DFT studies of two pentacoordinated zinc (II) complexes containing quinazoline and 1, 10-phenanthroline as mixed ligands. *J. Lumin.* **2018**, *203*, 234–246. [CrossRef]
76. Purkayastha, A.; Debnath, D.; Majumder, M.; Ortega-Castro, J.; Kirillov, A.M.; Ganguly, R.; Misra, T.K. Nickel (II) based homo- vs heterometallic 1D coordination polymers derived from a novel 6-aminouracil building block: Structures, topologies, non-covalent interactions, magnetism, and antibacterial activity. *Inorg. Chim. Acta* **2018**, *482*, 384–394. [CrossRef]
77. Tabong, C.D.; Yufanyi, D.M.; Paboudam, A.G.; Nono, K.N.; Eni, D.B.; Agwara, M.O. Synthesis, crystal structure, and antimicrobial properties of [diaquabis(hexamethylenetetramine)diisothiocyanato-κN]nickel (II) complex. *Adv. Chem.* **2016**, 1–8. [CrossRef]
78. Colinas, I.R.; Rojas-Andrade, M.D.; Chakraborty, I.; Oliver, S.R.J. Two structurally diverse Zn-based coordination polymers with excellent antibacterial activity. *CrystEngComm* **2018**, *20*, 3353–3362. [CrossRef]
79. Rauf, A.; Ye, J.; Zhang, S.; Shi, L.; Akram, M.A.; Ning, G. Synthesis, structure and antibacterial activity of a copper (II) coordination polymer based on thiophene-2,5-dicarboxylate ligand. *Polyhedron* **2019**, *166*, 130–136. [CrossRef]